First synthesized WS_2 nanotube and nanoribbon field effect transistors grown by chemical vapor transport

Sara Fathipour[1], Huamin Li[1], Paolo Paletti[1], Maja Remškar[2],
Susan Fullerton-Shirey[3], and Alan Seabaugh[1]
[1]*Dept. of Electrical Engineering, Univ. of Notre Dame, Notre Dame, IN 46556, USA*
[2]*Jožef Stefan Institute, Ljubljana, Slovenia*
[3]*Univ. of Pittsburgh, Dept. of Chemical and Petroleum Eng., Pittsburgh, PA 15213, USA*
Email: sfathipo@nd.edu, seabaugh.1@nd.ed / Phone: (574) 631-4473

Introduction. While planar two-dimensional field effect transistors (FETs) are being widely explored [1], there are only a few reports of MoS_2 [2-4] and WS_2 [5-8] nanotube (NT) and nanoribbon (NR) FETs. A benefit of these crystalline forms is the absence of edges associated with traps, and the potential for ideal subthreshold swing with wrapped gates. Density functional theory predicts that the bandgap of MoS_2 nanotubes remains direct and decreases with diameter [9] due to strain. This makes nanotubes appealing for tunnel FETs at the scaling limit because the decrease in bandgap should provide an increase in current. Here we report the first WS_2 NT and NR FETs synthesized by chemical vapor transport (CVT) [10]. Prior reports on WS_2 [5-8] are based on sulphurization of W and WO nanowhiskers.

Device Results. We show ON/OFF ratios as high as 6×10^4 which is higher than all prior reports on WS_2 FETs. FETs with Ti/Au contacts (5 nm/120 nm) showed a stronger *n*-branch and devices with Ti/Pd contacts (0.7 nm/120 nm) showed a stronger *p*-branch. On completion, the highest measured channel current was 3.6 µA/µm at $V_{DS} = 2$ V. The FETs were then ion doped both *n*-type and *p*-type by drop casting the solid polymer, polyethylene oxide cesium perchlorate (PEO:$CsClO_4$). Side gates were used to position the mobile Cs^+ and ClO_4^- ions to form electric double layers (EDLs) for doping of the FET channels. A current density of 114 mA/µm^2 at 80 K, 104 mA/µm^2 at 110 K and 100 mA/µm^2 at 140 K was achieved at $V_{DS} = 0.8$ V and $V_{SG} = 4$ V for the *n*-doping case. The current at room temperature could then be extrapolated to be 63 mA/µm^2 with an approximate contact resistance of 380 Ω µm. A current density of 0.76 mA/µm^2 at 110 K, 0.86 mA/µm^2 at 140 K and 0.91 mA/µm^2 at 170 K was achieved at $V_{DS} = -2.4$ V and $V_{SG} = -4.5$ V for the *p*-doping case with the current at 300 K extrapolated to be 1.24 mA/µm^2.

Growth and Fabrication. The WS_2 nanostructures were grown by the CVT method from a WS_2 powder source, using iodine as the transport agent in an evacuated silica ampoule. CVT allows the growth of the NTs with lower structural defects as compared to the sulfurization method [2]. Some nanotubes collapse during the growth and take on a nanoribbon form. The FET process flow consisted of electron beam evaporation of Ti/Au (5 nm/100 nm) on the back of a p^+ Si wafer. Al_2O_3 (27 nm) was deposited by atomic layer deposition to form the back-gate oxide. CVT grown WS_2 NTs and NRs were tape transferred onto the Al_2O_3 and source, drain and side gate contacts were patterned using electron beam lithography. Two types of metal contacts were deposited as the source/drain metal contact: Ti/Au (5 nm/ 120 nm) and Ti/Pd (0.7 nm/ 120 nm). Palladium and Ti were chosen as high and low work function metals, respectively. Polyethylene oxide and $CsClO_4$ were dissolved in anhydrous acetonitrile, drop-cast onto the wafer and annealed at 90 °C. The ions are mobile at room temperature in the electrically insulating solid polymer. To lock the doping, the device is cooled below the glass transition temperature of the electrolyte, 244 K, while continuously applying the bias on the side gate contact. Details of this approach are published [11-13]. Current-voltage measurements were performed in a Cascade PLC50 vacuum probe station at 1.2×10^{-6} Torr.

Physical Characterization. Raman spectroscopy was performed in a back scattering configuration using a WITec Alpha 300 system at room temperature (100× objective, 488 nm laser wavelength, and 0.5 mW power). Clear Raman in-plane vibrational mode (E^1_{2g}) and out-of-plane vibrational mode (A_{1g}) for WS_2 were detected. Transmission electron microscopy of the tested FETs provide unambiguous dimensional confirmation.

Acknowledgements. This research was funded in part by TSMC. The authors would like to thank L. Yeh, W. Tsai, Y. Lin, and E. Chen for useful discussions. **References**. [1] Fiori *et al., Nature Nanotech.* 9, 768 (2014)]. [2] M. Remškar *et al., Nanoscale Res. Lett.* 6, 26 (2011). [3] M. Strojnik *et al, AIP Adv.* 4, 097114 (2014). [4] S. Fathipour *et al., Appl. Phys. Lett.*, 106, 022114 (2015). [5] R. Levi *et al., Nano Lett.* 13, 3736 (2013). [6] H. E. Unalan *et al, IEEE TED* 55, 2988 (2008). [7] M. Sugahara *et al, Appl. Phys. Expr.* 9, 075001 (2016). [8] H. Kawai *et al. Appl. Phys. Expr.* 015001 (2017). [9] Seifert *et al., Phys. Rev. Lett.* 85, 146 (2000). [10] M. Remškar *et al. Appl Phys. Lett.* 69, 351 (1996). [11] H. Xu *et al. ACS Nano* 9, 4900 (2015). [12] S. Fathipour *et al. J. Appl. Phys.* 120, 234902 (2016). [13] S. Fathipour *et al. 2016 VLSI-TSA*.

978-1-5090-6328-4/17/$31.00 ©2017 IEEE

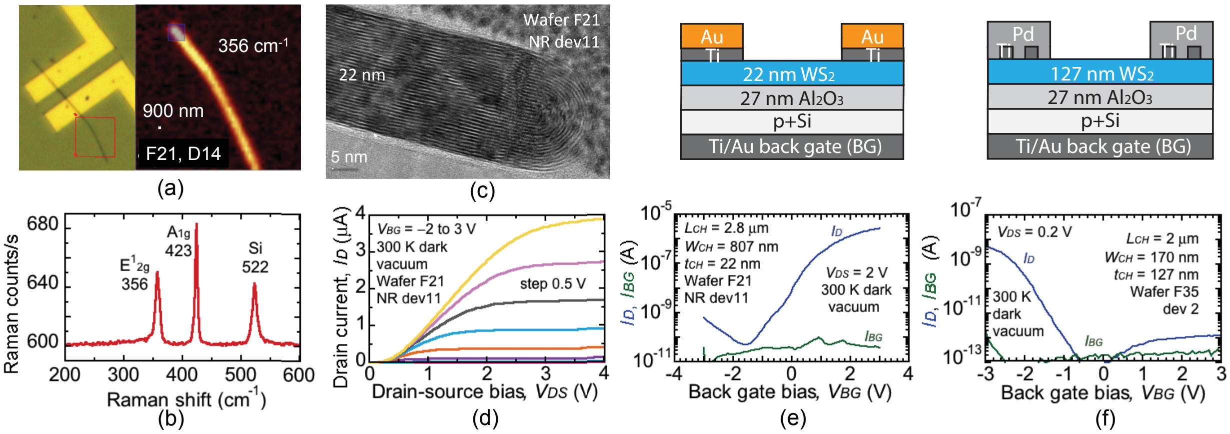

Fig. 1. (a) Raman mapping on CVT grown WS_2 for the E^1_{2g} mode. The left figure shows the optical image of the WS_2 NT. The mapping region is shown with a red square. **(b)** Raman spectrum of WS_2 NT taken with a 100× objective, 488 nm laser wavelength, and 0.5 mW power. **(c)** TEM image of a WS_2 NR; wrapping of the edge of the ribbon is observed. **(d)** Common source characteristics of the WS_2 NR FET with the TEM cross-section shown in (c). **(e)** Top figure; schematic cross section of the WS_2 FET when Ti/Au (5 nm/120 nm) is deposited as source/drain contact. Bottom figure; transfer characteristics for the Ti/Au contact device. Device shows a stronger *n*-branch with Ti/Au contact. **(f)** Top figure; schematic cross section of the WS_2 FET when Ti/Pd (0.7 nm/120 nm) is deposited as source/drain contact. Bottom figure; transfer characteristics for the Ti/Pd contact device. Device shows a stronger *p*-branch with Ti/Pd contact.

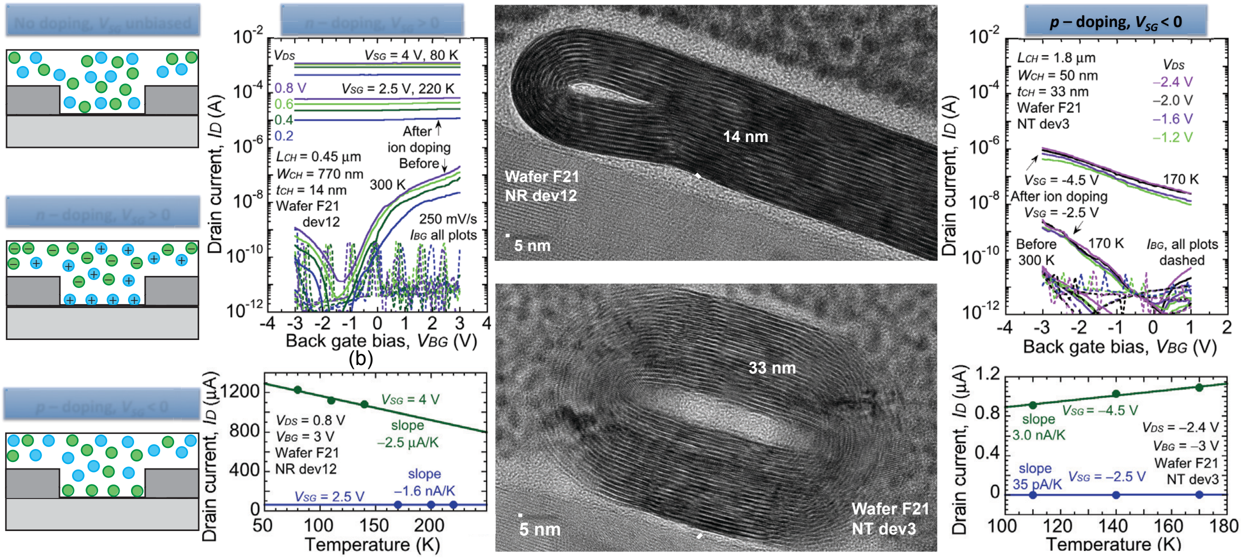

Fig. 2 (a). Schematic of the EDL *n*-doping and *p*-doping mechanisms formed by a side gate (not shown). Top figure; when there is no bias applied to the side gate the ions are homogenously distributed in the electrolyte. Middle figure, applying a positive voltage on the side gate positions Cs^+ ions on the channel and dopes the device *n*-type. Bottom figure, applying a negative voltage on the side gate positions the ClO_4^- ions on the channel and dopes the device *p*-type. **(b)** Transfer characteristics before and after EDL *n*-doping with two different side gate biases, 2.5 and 4 V. After EDL doping the threshold voltage shifts towards more negative values, ON-current increases and gate modulation decreases, showing that the *n*-doping was effective. **(c)** Temperature dependence of the drain current on a linear scale at V_{SG} of 2.5 and 4 V. Extrapolating the current at V_{SG} = 4 V to 300 K indicates a high current density of 63 mA/µm^2 at V_{DS} = 0.8 V. **(d)** TEM of the WS_2 nanoribbon with the characteristics shown in (b) and (c). **(e)**. TEM image of the WS_2 nanotube with the characteristics shown in (f) and (g). **(f)** Transfer characteristics before and after EDL *p*-doping with two different side gate biases, –4.5 and –2.5 V. After EDL *p*-doping, the threshold voltage shifts toward more positive values. **(g).** Temperature dependence of the drain current on a linear scale at V_{SG} of −2.5 and −4.5 V. Extrapolating the current at $V_{SG} = -4.5$ V to 300 K gives 1.24 mA/µm^2 at $V_{DS} = -2.4$ V.

978-1-5090-6328-4/17/$31.00 ©2017 IEEE